International Journal of Computer Information Systems and Industrial Management Applications
ISSN 2150-7988 Volume 18(8s) 2026 pp. 492-510
https://doi.org/10.70917/ijcisim-2026-3292
Article

RUMS-net: A Deep Learning Framework for Accurate Segmentation and Classification of Lung Cancer Images

Ankala Radhika[1]*, Pravin kulurkar[2] ,PravinRamdas Kshirsagar[3] , k.Aanandha saravanan [4] , M.Latha [5,] M Baby Nitmala[6]

[1]Department of Computer Science and Engineering, SRK Institute of Technology, Vijayawada-521108, AndhraPradesh, India. radhikaankala@gmail.com
[2]Department of Computer science and Engineering, J D College of Engineering & Management Nagpur, pravinkulurkar@gmail.com
[3]J D College of Engineering & Management, Nagpur, INDIA, prkshirsagar@jdcoem.ac.in
[4]Dept of ECE,VelTech Rangarajan Sakunthala R & D Institute of science & Technology, Avadi, Chennai – 62 , aanandhasaravanan@veltech.edu.in
[5]Department of Information Technology, SRM institute of Science and technology,Ramapuram , latham@srmist.edu.in
[6]Dept of Computer science and Engineering, Dhanalakshmi Srinivasan University, Tiruchirappalli,Tamilnadu babynirmalam.mca@dsuniversity.ac.in

Abstract: This study gives a precise methodology to accurately process and classify thoracic cancer images using the The Lung Image Database Consortium image collection dataset. Given proposed approach utilizes the RUMS-net model, which combines ResNet-50, U-Net, and Multi-Class SVM algorithms. The process commences by resizing images utilizing bicubic interpolation, subsequently applying bilateral filtering to diminish noise while maintaining edges. Contrast enhancement is accomplished through the use of Bi-Histogram Equalization with Brightness Preservation Technique (BBHE), and the input image is then transformed to a binary format using an iterative selection thresholding method. The binary image is refined through morphological opening operations using disk-shaped structuring elements. Subsequently, the refined image is inverted and utilized for active contour segmentation employing the Random Walker algorithm. The inverted images are overlaid with segmented contours, and then Wiener filtering is implemented. The image undergoes a conversion to binary, followed by hole filling. Circle detection is then used to identify regions of interest, which are overlaid onto the original image. The segmented image is obtained through the subtraction of binary images, and quantitative metrics such as the total area of the tumor and the ratio of affected area are calculated. The RUMS-net model utilizes ResNet-50 for feature extraction, U-Net for segmentation, and Multi-Class SVM for classification in order to perform classification. The proposed model attains 99.75% as accuracy rate, sensitivity of 99.91%, 98.23% specificity, and precision of 99.79%, surpassing other models and showcasing its effectiveness in delivering accurate and dependable medical diagnosis and analysis.

Keywords: Lung cancer, random Walker, Histogram, Deep learning , SVM, circle, weiner, Thresholding.

1. Introduction

Lung cancer prevails as a prominent oncogenic cause of fatalities globally, presenting substantial health hazards to millions of individuals. The main cause of the disease is smoking, and is responsible for around 85% of cases [1-3]. However, non-smokers can also develop the disease due to factors such as radon gas exposure also due to other cancer-causing substances [4-6]. The disease progresses gradually and often does not show any symptoms until it reaches advanced stages, which makes it difficult to detect in its early stages. The Global Health Organization (WHO) reports that this type of cancer causes 1.8 million deaths each year, highlighting the pressing need for enhanced diagnostic and therapeutic approaches. Lung carcinoma is categorized to two primary types: non-small cell and small cell cancer . The prior type of cancer which is NSCLC, comprising squamous cell carcinoma, adenocarcinoma,

and large cell carcinoma, are the predominant cause for 85% of all cases. These categories vary in terms of their cellular source, patterns of growth, and tendency to progress and affect other parts of the body [7-10]. Lung cancer originates in the lungs but has the ability to metastasize, spreading to lymph nodes, the brain, liver, bones, and other organs [11-15]. This widespread dissemination greatly complicates the process of treating the condition and diminishes the chances of survival, underscoring the criticality of prompt and precise diagnosis [16-18].

The approach to diagnosing and classifying lung cancer has been revolutionized by recent advancements in medical imaging and artificial intelligence [19]. Convolutional neural networks (CNNs) have been widely used in medical imaging due to their capacity to automatically extract and analyze intricate features from images. These methods have proven potential in increasing the precision and accuracy of identifying, dividing, and categorizing lung cancer, consequently enhancing the overall results in clinical settings. The fusion of deep learning and conventional image processing methods offers a potent instrument for medical practitioners in their fight against lung cancer. This study introduces an innovative approach to analyse and categorize lung carcinoma images using the RUMS-net model. This model utilizes the advantages of ResNet-50 for extracting features, U-Net for segmenting, and Multi-Class SVM for classifying. The initial steps of our approach involve preprocessing, which includes resizing, reducing noise, and enhancing contrast. This is followed by employing advanced segmentation techniques and conducting quantitative analysis. The RUMS-net model demonstrates exceptional performance metrics, with 99.75% accuracy, 99.91% sensitivity, 98.23% specificity, and 99.79% precision. This showcases its effectiveness in delivering accurate and dependable medical diagnosis and analysis.

The organization of this work is structured as follows: The Introduction of work is provided in Section 1. Section 2 reviews current methodologies and their constraints. Section 3 provides an explanation of the proposed system, and the RUMS-net model. Section 4 showcases the empirical findings, encompassing performance metrics. Section 5 serves as the concluding part of the paper, providing a summary of the findings.

2. Literature Review

In 2024, Zhang et al. [20] employed a DenseNet-based CNN to find thoracic cancer. They achieved 99% impressive accuracy, 0.998 recall, and precision of 0.992. These results demonstrate the network's ability to accurately identify lung cancer cases and minimize false positives. Nevertheless, the model's high complexity could lead to potential overfitting, which may hinder its ability to generalize to unseen data. Parveen et al. [21] introduced a technique called ensemble model that combines multiple 2D CNN architectures to diagnose lung cancer. Their model has acquired 91% accuracy rate , a sensitivity rate of 82.4%, and a 93.9% specificity rate. This approach demonstrated potential in utilizing the capabilities of various CNN models to enhance diagnostic accuracy. Nevertheless, the heightened computational expense and intricacy of the ensemble method may present obstacles in real-time clinical implementations. In 2024, Nair et al. [22] gave a hybrid model that collaborates the Random Walker algorithm with Random Forest classifiers to detect lung cancer. Their approach demonstrated an exceptional level of accuracy, with a rate of 99.6%. Additionally, it achieved a specificity of 94.7% and a precision of 99.7%. This was accomplished by effectively combining segmentation and classification techniques, resulting in improved diagnostic accuracy. Nevertheless, the high level of computational complexity and the requirement for meticulous parameter adjustment may restrict its feasible application.

In a separate study conducted in 2024, Venkatesh et al. [23] created a hybrid model utilizing Convolutional Neural Networks (CNN) to detect lung cancer. The study reported 99% an accuracy rate, 98.5% sensitivity rate, and 61% a specificity rate. Although the model demonstrated high accuracy and sensitivity, its relatively low specificity suggests a higher incidence of false positives, potentially resulting in unnecessary follow-up procedures and causing patient distress.

In 2024, Krishna and colleagues [24] presented a model for diagnosing lung cancer by combining a decision tree (DT) with a VGG model. Their method yielded an accuracy rate of 92.53%, 97% sensitivity, and a precision rate of 94%. This model successfully achieves a harmonious combination of basic decision trees and advanced deep learning features derived from VGG. Nevertheless, the limitations of decision trees, such as potential overfitting, and the difficulty of seamlessly integrating two distinct model architectures, still persist. In 2024, Chu et al. [25] utilized the Xception model to detect lung cancer. They reported an accuracy of 96.3%, precision of 94.8%, recall of 98.0%, F1 score of 96.4%, AUC of 99.4%, and specificity of 94.7%. The Xception model's impressive performance across multiple metrics highlights its resilience, but its intensive computational requirements and intricate nature may impede its implementation in settings with limited resources.

In 2023, Nazir et al. [26] proposed a multi-view fusion technique for detecting lung cancer, which achieved an accuracy rate of 98.2% and a sensitivity rate of 96.4%. This method efficiently combines information from multiple perspectives to improve diagnostic precision. Nevertheless, the growing need for data processing and the intricate nature of integrating multi-view data may hinder its ability to scale.

In 2023, Rajasekar et al. [27] introduced a convolutional neural network (CNN) that utilized gradient descent optimization to detect lung cancer. Their approach achieved 97.86% accuracy, 96.39% precision, 96.79% sensitivity, and 97% specificity. This approach leverages the effective optimization of gradient descent, enhancing the performance of the model. Nevertheless, the presence of local minima traps in gradient descent may impact the model's convergence and accuracy.

In 2023, Rajput et al. [28] achieved a 98.57% accuracy rate for their lung cancer detection model. While the high accuracy of the study suggests that it performs well, it does not provide sufficient information on other important metrics like sensitivity, specificity, and precision. This lack of detail makes it difficult to fully evaluate the reliability of the model and identify any potential limitations.

To summarize, different methodologies have been investigated for the identification of lung cancer, with each demonstrating encouraging outcomes in terms of precision and other evaluative criteria. Nevertheless, prevalent constraints encompass the possibility of overfitting, the computational intricacy, and the necessity for thorough parameter adjustment, all of which may influence the practical application and universality of these models.

3. Proposed System

The proposed methodology in Fig. 1 entails a thorough pipeline for image processing and analysis in medical imaging, specifically utilizing the LIDC-IDRI dataset. The procedure commences by importing an image and adjusting its dimensions to a uniform size of 256x256 pixels through the utilization of bicubic interpolation. The application of bilateral filtering reduces noise while maintaining the sharpness of edges. This is then followed by BBHE (Brightness Biased Histogram Equalization) for enhancing contrast. The image is subsequently transformed into binary format utilizing a dynamic threshold, followed by the execution of morphological opening operations with varying radii. The binary image is subjected to active contour segmentation using the Random Walker algorithm, followed by Wiener filtering and additional binarization. Circle detection is employed to identify specific areas of interest, and the resulting binary image is produced by subtracting two binary images and applying a threshold. Quantitative measurements, such as the overall tumor area and the ratio of affected tissue, are computed. The RUMS-Net model, which combines ResNet-50, U-Net, and Multi-Class SVM, is employed to extract features, perform segmentation, and carry out classification, thereby ensuring a strong and accurate medical diagnosis.

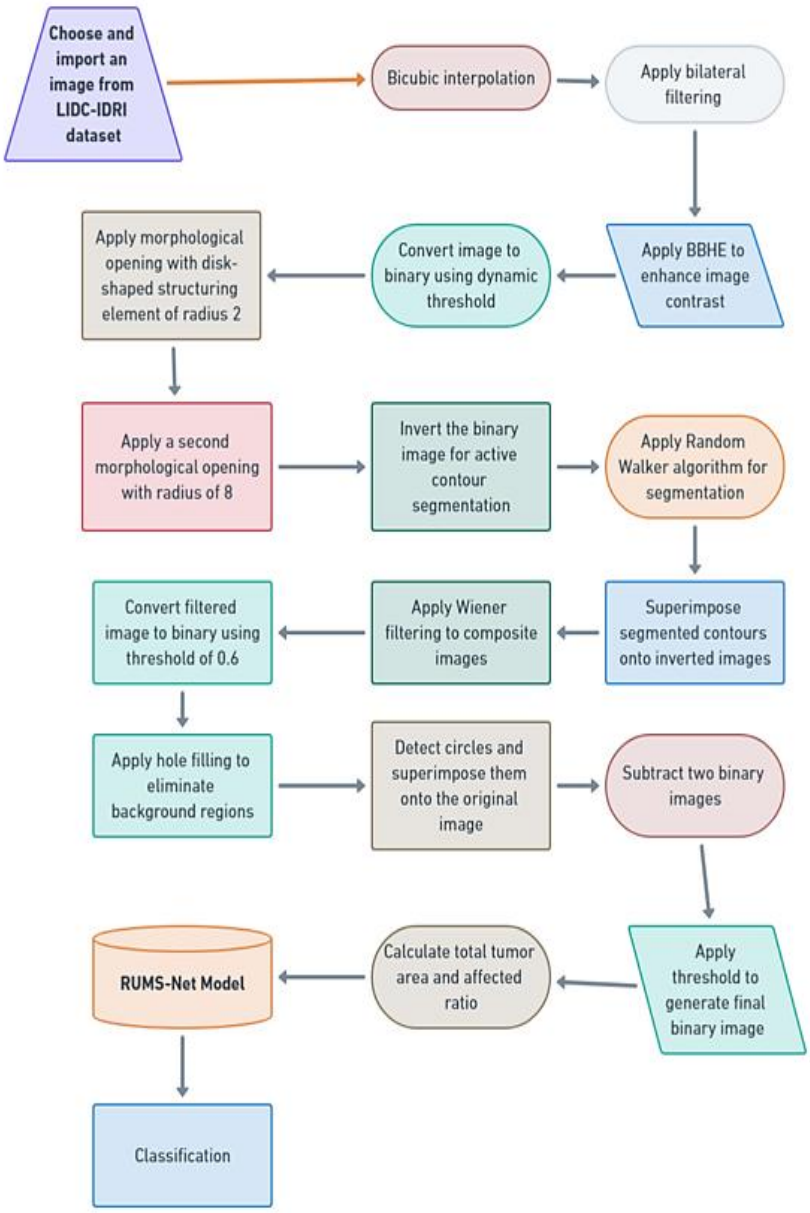

Fig. 1 Proposed Block Diagram for Lung Cancer Detection

The methodology commences by choosing and importing an image from the LIDC-IDRI dataset.

After the image is loaded, it is resized to a consistent size (such as 256x256) using bicubic Resize I to 256 × 256 using bicubic interpolation

$$I_{resized} = resize(I, 256{,}256) \quad \text{.....(1)}$$

interpolation to ensure uniformity in the following processing stages.

Resizing the input dimensions is essential for ensuring consistent processing and analysis by standardizing them.

Subsequently, the resized image undergoes bilateral filtering. Bilateral filtering is a highly effective technique for reducing noise in medical imaging while also preserving crucial edge information.

Apply bilateral filtering to reduce noise while preserving edges:

$$I_{filtered}(x,y) = \frac{1}{W(x,y)} \sum_{x_i,y_i} \quad I_{resized}(x_i,y_i).\, e^{-\frac{(x-x_i)^2+(y-y_i)^2}{2\sigma_d^2}} .\, e^{-\frac{(I_{resized}(x,y)-I_{resized}(x_i,y_i))^2}{2\sigma_r^2}} .(2)$$

where W(x, y) is a normalization factor.

This is essential for maintaining the accuracy and integrity of anatomical structures. After reducing the noise, the BBHE (Bi-Histogram Equalization) method is used to improve the contrast of the image.

Apply BBHE to enhance image contrast:

$$I_{BBHE} = BBHE\ (I_{filtered}) \quad \text{.....(3)}$$

This step is crucial for enhancing the perceptibility of characteristics within the image, facilitating the distinction between different regions of interest.
The processed image is subsequently transformed into a binary format through the utilization of iterative selection thresholding.

Convert the image to binary using a dynamic threshold T:

$$T = \frac{1}{2}\ (\mu_{foreground} + \mu_{background}) \quad \text{.....(4)}$$

$$I_{binary}(x,y) = \{1\ \ If\ I_{BBHE}(x,y) \geq T\ 0\ \ If\ I_{BBHE}(x,y) < T \quad \text{.....(5)}$$

This approach utilizes a dynamic process to calculate the most suitable threshold value for binarization, effectively preserving crucial details while minimizing interference from background noise. Afterwards, a morphological opening operation is conducted using a structuring element which is disk-shaped with a radius of 2. This operation facilitates the elimination of minuscule entities and enhances the smoothness of the outlines of more substantial entities in the binary image.

In order to enhance the accuracy of the binary image, a morphological opening operation is applied using a larger structuring element with a radius of 8.

Apply morphological operation with a structuring element of radius 2:

$$I_{opened} = open\ (I_{binary,} disk(2)) \quad \text{.....(6)}$$

Apply a second morphological opening with a radius of 8:

$$I_{opened2} = open\ (I_{opened,} disk(8)) \quad \text{.....(7)}$$

This results in the creation of an inverted binary image. The inversion is essential for the active contour segmentation process.

Invert the binary image for active contour segmentation:

$$I_{inverted} = 1 - I_{opened2} \quad \text{.....(8)}$$

The Random Walker algorithm is subsequently utilized for active contour segmentation on the inverted binary images. This algorithm is efficient in determining the boundaries of objects based on pixel intensity, yielding precise segmentation outcomes.

$$I_{segmented} = Random\ Walker\ (I_{inverted}) \quad \text{.....(9)}$$

Combination images are formed by superimposing the segmented contours onto the inverted images, and then applying Wiener filtering to minimize noise in these composite images.

Superimpose segmented contours onto inverted images:

$$I_{combined} = I_{segmented} + I_{inverted} \quad \text{.....(10)}$$

Apply Wiener filtering to $I_{combined}$:

$$I_{Wiener} = WeinerFilter(I_{combined}) \quad \text{.....(11)}$$

The filtered composite images are subsequently transformed into binary format by applying a threshold value of 0.6. Hole filling is applied to the binary image to eliminate any background regions, ensuring that only the regions of interest are preserved.

Convert I_{Wiener} to binary using a threshold of 0.6:

$$I_{binary2}(x,y) = \{1 \ \ If \ I_{Wiener}(x,y) \geq 0.6 \ 0 \ \ If \ I_{Wiener}(x,y) < 0.6 \quad \text{.....(12)}$$

Apply hole filling to $I_{binary2}$:

$$I_{filled} = HoleFillinh(I_{binary2}) \quad \text{.....(13)}$$

The segmented image is subjected to circle detection in order to identify potential regions of interest, such as tumors. The identified circular shapes are superimposed on the original image to enhance visual representation.

Detect circles in f_filled and superimpose them onto the original image:

$$I_{Circles} = CircleDetection\ (I_{filled}) \quad \text{.....(14)}$$

Superimpose:

$$I_{final} = I + I_{Circles} \quad \text{.....(15)}$$

The segmented image is computed by subtracting two binary images, and a threshold is then applied to generate a final binary image.

Subtract two binary images:

$$I_{Subtracted} = I_{binary2} - I_{binary} \quad \text{.....(16)}$$

Using a threshold to form the binary image:

$$I_{final\ binary} = \{1 \ \ If \ I_{subtracted} \geq T \ 0 \ \ If \ I_{subtracted} < T \quad \text{.....(17)}$$

Quantitative metrics for analysis are derived from the segmented image, including the total tumor area and affected ratio. The classification of the tumor is established according to these metrics.

Calculate the total tumor area A_{tumor} and affected ratio $R_{affected}$:

$$A_{tumor} = \sum_{x,y} \quad I_{final\ binary}(x,y) \quad \text{.....(18)}$$

$$R_{affected} = \frac{A_{tumor}}{Total\ Area} \quad \text{.....(19)}$$

RUMS-Net, a sophisticated model that combines ResNet-50, U-Net, and Multi-Class SVM, is ultimately employed for classification. This model utilizes the capabilities of ResNet-50 for extracting features, U-Net for segmenting, and Multi-Class SVM for classifying.

Extract features USING RasNet-50:

$$F_{RasNet} = RasNet50(I) \text{ .....(20)}$$

Segmentation using U-Net:

$$S_{U-Net} = U - Net(F_{RasNet}) \text{ .....(21)}$$

Classify using MultiClass SVM:

$$C_{svm} = MultiClassSVM(S_{U-Net}) \text{ .....(22)}$$

Features are derived from the training images, and the model is then trained using these derived features. The performance of the classifier is assessed, and the outcomes are displayed to gain understanding of the accuracy and effectiveness of the classification. This comprehensive methodology guarantees strong image processing, segmentation, and classification, which are essential for precise medical diagnosis and analysis.

3.1 Proposed Model RUMS-Net Model

The term RUMS-Net represents the fundamental elements and the fundamental nature of the merged model, which combines ResNet-50 for in-depth feature extraction, U-Net for accurate segmentation, and Multi-Class SVM for strong classification. Every element in the title represents a vital aspect of the model, guaranteeing lucidity and emphasizing the innovative fusion of these potent techniques. This terminology not only makes it easy to refer to, but also highlights the distinctive combination of these sophisticated structures, making it suitable for both academic and practical discussions.

The design of RUMS-Net as given in Figure 2 capitalizes on the capabilities of ResNet-50, U-Net, and Multi-Class SVM to attain exceptional results in intricate assignments. The model starts with the ResNet-50 backbone, which consists of several residual layers (from Conv1 to Conv5_x). These blocks effectively extract deep hierarchical attributes. The extracted features are subsequently inputted into the U-Net architecture, which comprises an encoder path (contracting path) with convolutional and max-pooling layers, as well as a decoder path (expanding path) with up-convolution and concatenation layers. The U-Net architecture consists of Down1 to Down5 layers for the encoding process and Up1 to Up5 layers for the decoding process. Ultimately, the extracted and segmented features are fed into the Multi-Class SVM classifier, which classifies the data into separate categories. The overall architecture guarantees meticulous feature extraction, exact segmentation, and precise classification.

RUMS-Net presents an innovative approach that combines ML and DL methods to address intricate classification and segmentation challenges. ResNet-50 utilizes a residual learning framework to achieve effective and efficient feature extraction. This framework addresses the issue of the diminishing gradient problem and enables the training of highly complex networks. The inclusion of U-Net improves the model's capacity to capture intricate details by utilizing its encoder-decoder structure with skip connections, which preserve essential spatial information necessary for segmentation tasks. The inclusion of Multi-Class SVM introduces a strong classification method that excels in differentiating between multiple classes, relying on the complex feature representations acquired by the preceding layers. The smooth incorporation of these elements not only enhances efficiency but also showcases a notable progress in merging convolutional neural networks with conventional machine learning classifiers.

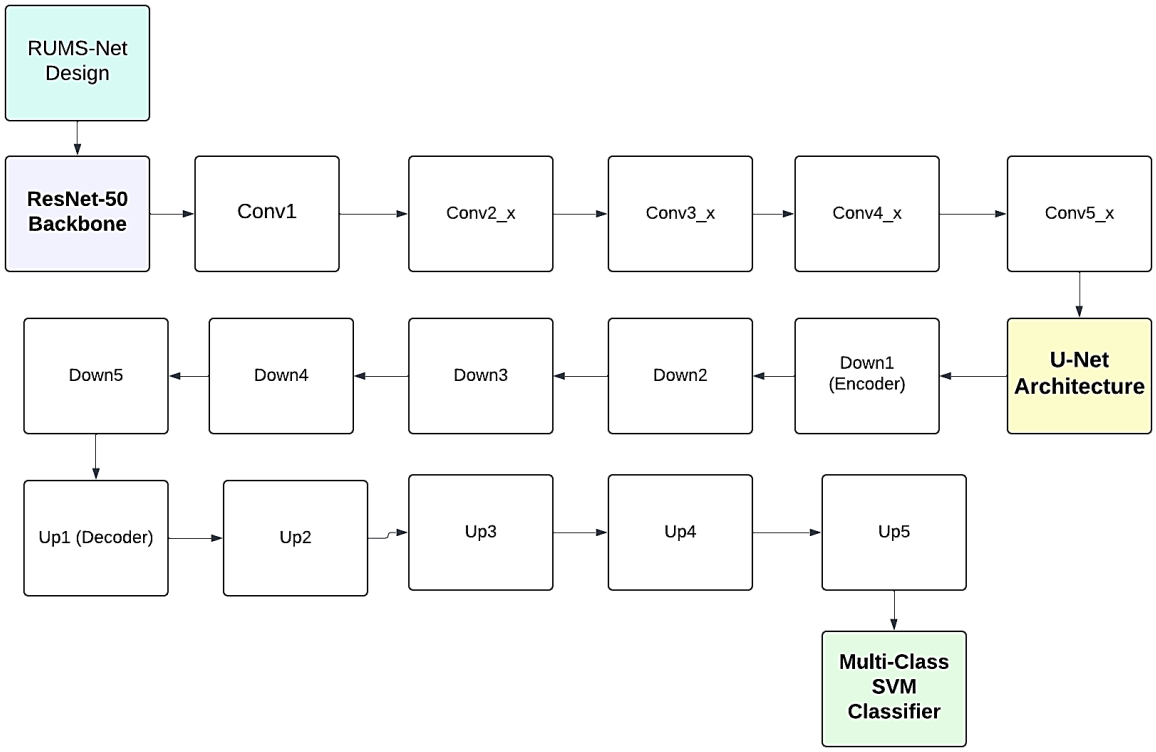

Fig. 2 Proposed RUMS-Net Architecture

3.2 Algorithm of the Proposed Model

The RUMS-Net algorithm utilizes the synergistic integration of ResNet-50, U-Net, and Multi-Class SVM to identify and categorize lung cancer from medical imaging data. The ResNet-50 backbone initially extracts deep, hierarchical features from the input lung images, capturing intricate details that are crucial for precise analysis. The U-Net structure processes these features, effectively dividing the images into significant regions and emphasizing potential areas of interest, such as tumors or nodules. The segmentation process entails utilizing an encoder path to get features and a decoder path to accurately locate abnormalities. Ultimately, the segmented characteristics are compressed and categorized using a Multi-Class Support Vector Machine (SVM), differentiating between non-cancerous and cancerous instances, and various types. The integration of various methods in RUMS-Net guarantees thorough extraction of features, accurate division into segments, and precise categorization, thereby establishing RUMS-Net as a reliable and efficient tool to detect and classify lung cancer in clinical environments.

Algorithm: Proposed RUMS-Net Model

```
% Step 1: Feature Extraction with ResNet-50
function features = resnet50_backbone(input)
    % Initial convolutional layer
    x = conv1(input);
    % Residual blocks for deep hierarchical feature extraction
    x = conv2_x(x);
    x = conv3_x(x);
    x = conv4_x(x);
```

```
    x = conv5_x(x);
    features = x;
end
% Step 2: Segmentation with U-Net
function segmented_features = unet_segmentation(features)
    % Encoder path (contracting path)
    down1 = down1_layer(features);
    down2 = down2_layer(down1);
    down3 = down3_layer(down2);
    down4 = down4_layer(down3);
    down5 = down5_layer(down4);
    % Decoder path (expanding path)
    up1 = up1_layer(down5, down4);
    up2 = up2_layer(up1, down3);
    up3 = up3_layer(up2, down2);
    up4 = up4_layer(up3, down1);
    up5 = up5_layer(up4, features);

    segmented_features = up5;
end

% Step 3: Classification with Multi-Class SVM
function output = multi_class_svm(segmented_features)
    % Flatten the features
    flat_features = reshape(segmented_features, [], 1);

    % Apply Multi-Class SVM for classification
    svm_model = fitcecoc(flat_features, labels); % Assume 'labels' is predefined
    output = predict(svm_model, flat_features);
end
```

4. Results and Analysis

The LIDC-IDRI dataset offers vital information about lung nodules, as illustrated in Figure 3, which displays a representative image of a lung nodule. This image acts as the basis for the following processing stages. The process

of noise reduction, as shown in Figure 4, utilizes bilateral filtering to retain important edge details while removing unwanted noise. Ensuring the preservation of anatomical structures in the image is of utmost importance. The processed image is subjected to morphological operations to further enhance its features. Figure 5 depicts the image that has undergone morphology processing, emphasizing the enhanced clarity in distinguishing the structures within the lung. Subsequently, the binary image undergoes inversion, as depicted in Figure 6, in order to prepare it for active contour segmentation.

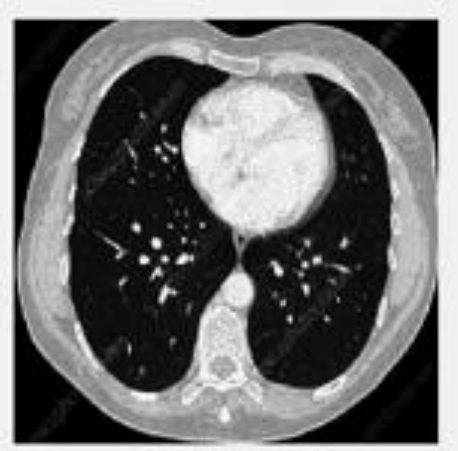

Fig. 3 Lung Nodule Sample Image

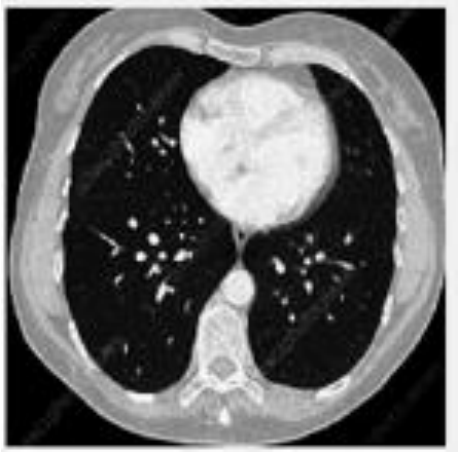

Fig. 4 Noise reduction

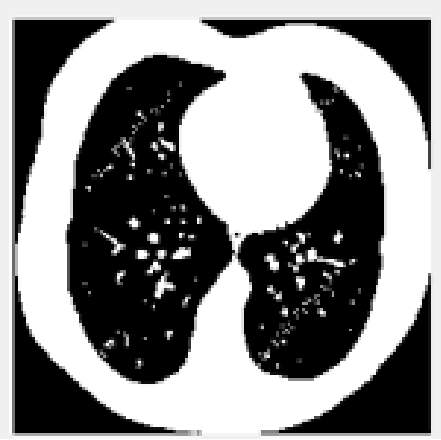

Fig. 5 Morphology processed Image

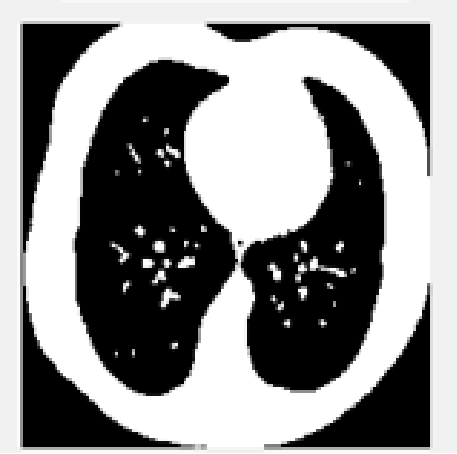

Fig. 6 Inverted Image

Segmentation is crucial for identifying distinct regions within an image. Figure 7 illustrates the segmented image, in which the boundaries of objects have been precisely identified. Subsequently, the image is readied for hole filling, as depicted in Figure 8. This process guarantees the elimination of any background regions, while specifically focusing on the regions of interest. The process of detecting circles, which is crucial for identifying potential tumors, is illustrated in Figure 9. The identified circular shapes are subsequently overlaid onto the original image, improving its visual depiction, as demonstrated in Figure 10. This method efficiently emphasizes areas of concern, enabling further analysis.

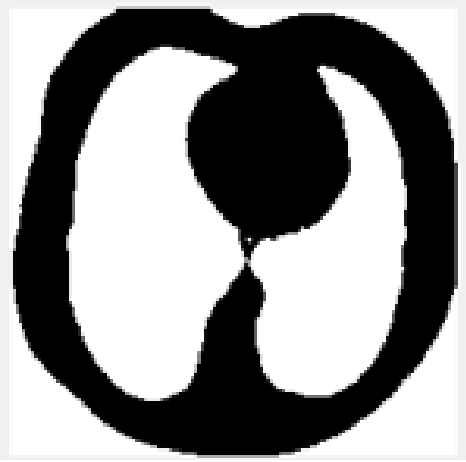

Fig. 7 Segmented Image

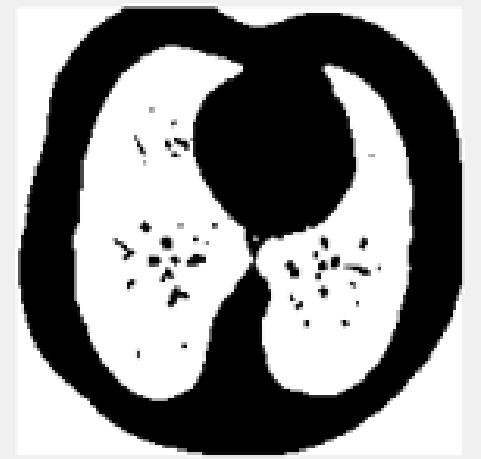

Fig. 8 Image ready for filling

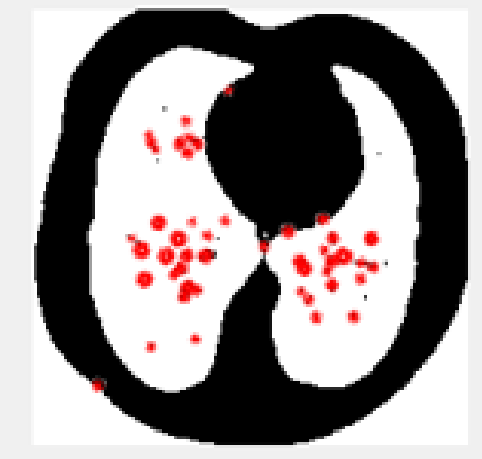

Fig. 9 Circle detection

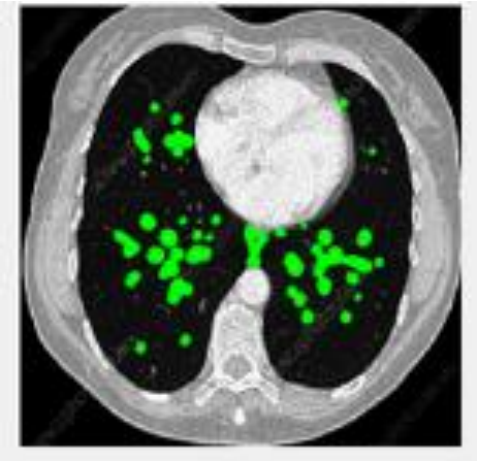

Fig. 10 Circles filled image

The detection process detected 52 circular shapes in the image, suggesting the existence of regions that may be cancerous. The significant number of identified circles strongly indicates a high likelihood of malignancy in the case.

In addition, the investigation examined cases categorized as low and medium severity. Within these specific categories, a total of 25 and 27 circles were accurately identified, respectively. Regarding the spatial extent of these identified circles, it is noteworthy that, for the high-cancer category, they collectively encompass an area of 2480 square pixels. By comparison, the low-cancer and medium-cancer types occupy 820 and 1150 square pixels, respectively. These measurements offer crucial data regarding the size and arrangement of cancerous lesions in the image.

The classification task, according to the proposed system, utilizes the LIDC-IDRI dataset, which is partitioned into training, validation, and testing subsets. The allocation of images among these subsets is essential for the efficient training, validation, and assessment of deep learning models in the field of medical image analysis. The dataset comprises a total of 1,200 images, which have been carefully categorized into four groups: Adenocarcinoma, Large Cell Carcinoma, Squamous Cell Carcinoma, and Normal Healthy Lung Images. The table below provides a comprehensive breakdown of the distribution of images among these categories and subsets.

Table 1. Category-wise distribution

Category	**Training**	**Validation**	**Testing**	**Total**
Adenocarcinoma	294	63	63	420

Large Cell Carcinoma	162	35	35	232
Squamous Cell Carcinoma	238	51	51	340
Normal Healthy Images	188	39	39	266
Total Images	882	188	188	1,200

The allocation of these categories is noteworthy as given in Table 1. Adenocarcinoma is the most common type, making up about 34.2% of all the images. The dataset consists of approximately 16.7% Large Cell Carcinoma images, 27.2% Squamous Cell Carcinoma images, and 21.9% Normal Healthy Lung images. These percentages demonstrate the relative distribution of each category, highlighting the dataset's diversity and significance in lung cancer research. The training subset comprises 70% of the total images, with 294 instances of Adenocarcinoma, 162 instances of Large Cell Carcinoma, 238 instances of Squamous Cell Carcinoma, and 188 instances of Normal Healthy Images. Both the validation and testing subsets consist of 15% of the entire collection of images. The validation dataset consists of 63 images of Adenocarcinoma, 35 images of Large Cell Carcinoma, 51 images of Squamous Cell Carcinoma, and 39 images of Normal Healthy tissue. Similarly, the testing subset exhibits an identical distribution to that of the validation subset.

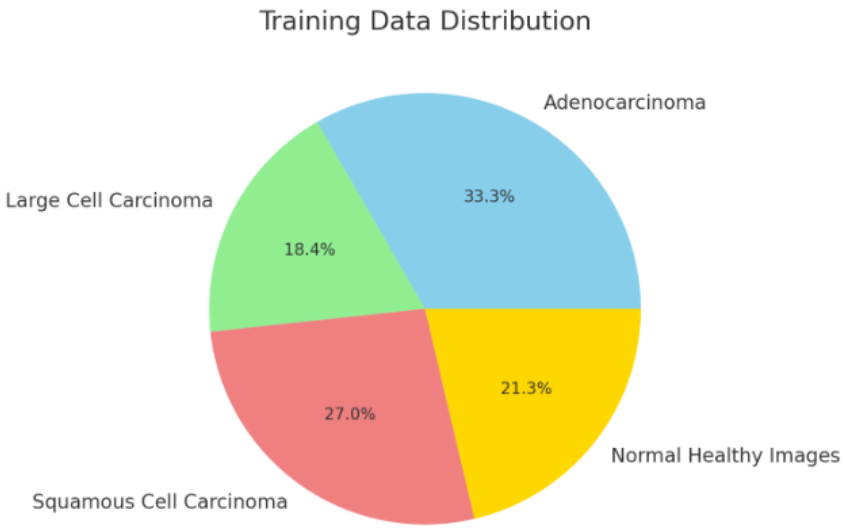

Fig. 11 Training Data Pie Chart

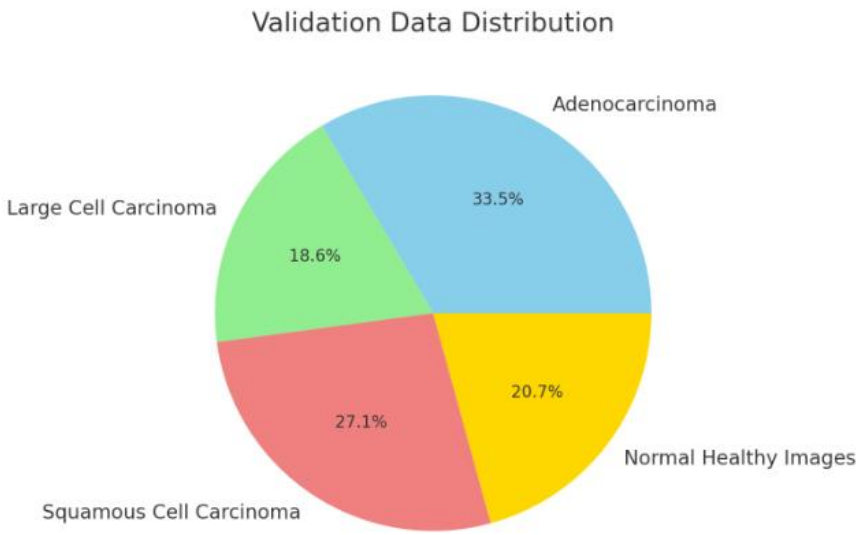

Figure 12. Validation data Pie chart

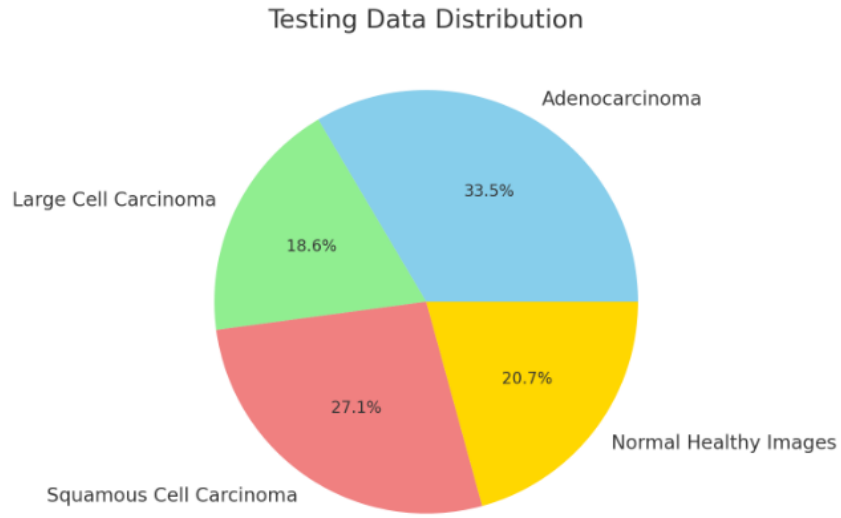

Fig. 13 Testing Data Pie chart

These distributions as shown in Fig. 11, 12 and 13 are critical in ensuring that the proposed RUMS-Net deep learning model is effectively trained, validated, and tested on a diverse and representative set of images. This careful categorization and proportional representation help in achieving robust and reliable models for lung cancer image analysis.

After loading the dataset, our developed model accurately classifies different types of lung cancer. Figure 14 illustrates a case of adenocarcinoma, whereas Figure 15 represents a squamous cell carcinoma. Figure 16 depicts a case of large cell carcinoma, while Figure 17 showcases a normal healthy case, allowing for a distinct comparison between malignant and non-malignant instances. Nevertheless, there are occurrences of misclassification, as depicted in Figure 18, where a typical case has been erroneously labeled as adenocarcinoma.

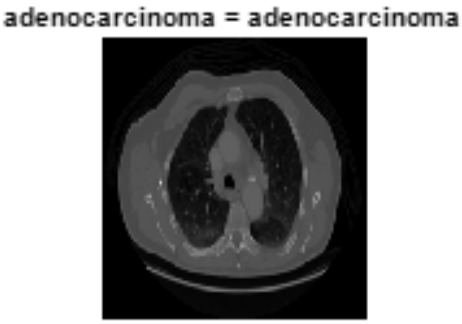

Fig.14 Adenocarcinoma Classified

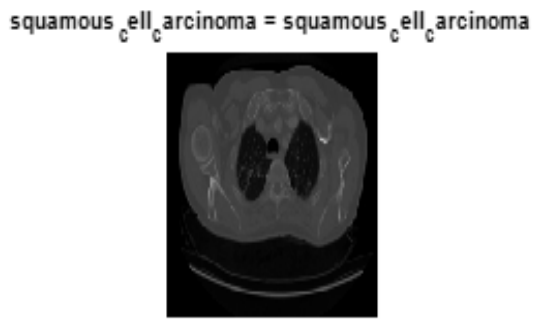

Fig. 15 Squamous Cell Carcinoma

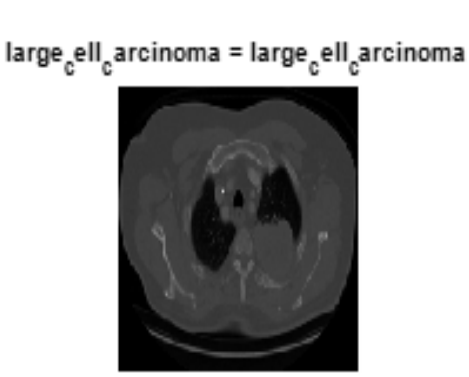

Fig.16 Large Cell Carcinoma

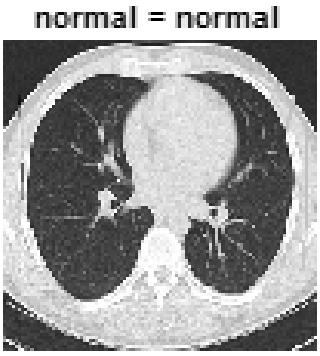

Fig. 17 Normal Healthy Case

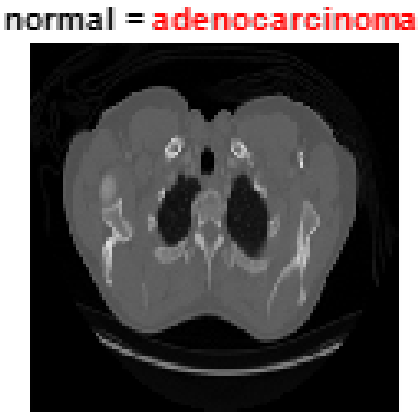

Fig. 18 Misclassification Case

(normal=adenocarcinoma)

Evaluate the classifier's performance using various metrics such as Accuracy, Specificity, Sensitivity and Precision.

4.1 Accuracy:

The percentage of correctly classified images is called as the Accuracy parameter and it is provided by equation (39).

$$Accuracy\ (ACC) = \frac{Number\ of\ Correct\ Predictions\ (CP)}{Total\ number\ of\ test\ samples\ (TN)}\ x\ 100 \ldots\ldots (23)$$

Sensitivity: The ability to correctly classify positive cases.

$$Sensitivity\ (SEN) = \frac{TP}{TP+FN} \ldots\ldots\ldots\ldots\ldots\ldots\ldots\ldots\ldots\ldots\ldots\ldots\ldots\ldots\ldots\ldots (24)$$

Specificity: The ability to correctly classify negative cases.

$$Specificity\ (SPEC) = \frac{TN}{TN+FP} \ldots\ldots\ldots\ldots\ldots\ldots\ldots\ldots\ldots\ldots\ldots\ldots\ldots\ldots\ldots\ldots (25)$$

Precision: The accuracy of positive predictions.

$$Precision\ (PREC) = \frac{TP}{TP+FP} \ldots\ldots\ldots\ldots\ldots\ldots\ldots\ldots\ldots\ldots\ldots\ldots\ldots\ldots\ldots\ldots (26)$$

TP - Number of true positives *FN* - number of false negatives.

The accuracy of various techniques is measured using accuracy metrics, as shown in Table 2. The accuracy of our proposed RUMS-net Model surpasses that of other models, achieving a remarkable 99.75%. Figure 19 presents a visual comparison of these accuracy metrics, illustrating the exceptional performance of our model.

Table .2 Accuracy Metrics

Method	Accuracy
DenseNet-CNN [20]	99.00
Ensembled 2D CNN [21]	91.00
Random Walker + Random Forest [22]	99.60
Hybrid Model CNN [23]	99.00
DT + VGG model [24]	92.53
Xception model [25]	96.30
Multi-view Fusion method [26]	98.20
CNN Gradient Descent [27]	97.86
CNN [Rajput et al. 28]	98.57
Proposed RUMS-net Model	99.75

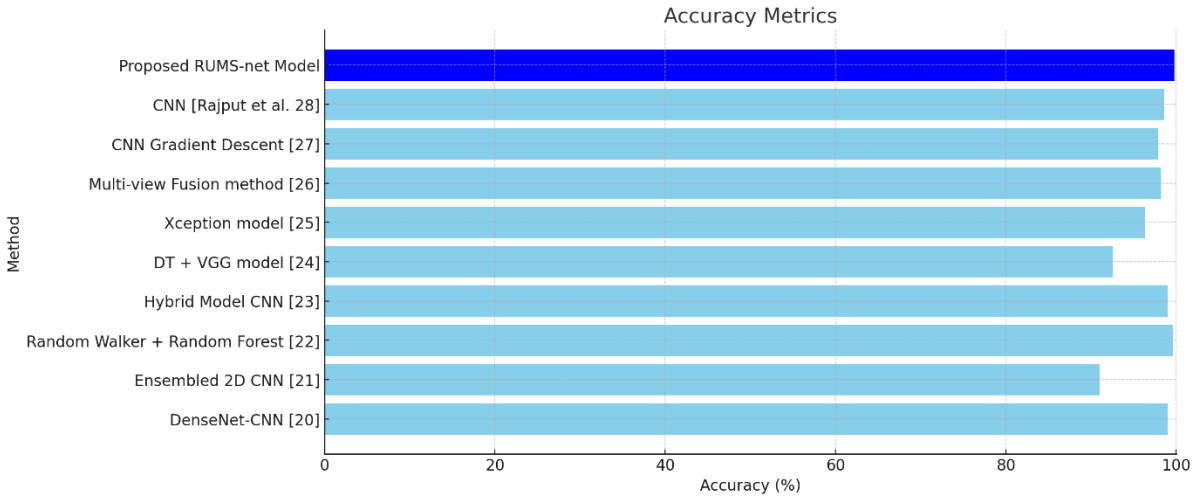

Fig. 19 Accuracy Comparison

Table 3 Sensitivity Metrics

Method	Sensitivity
DenseNet-CNN [20]	99.80
Ensembled 2D CNN [21]	82.40
Hybrid Model CNN [23]	98.50
DT + VGG model [24]	97.00
Xception model [25]	98.00
Multi-view Fusion method [26]	96.40
Proposed RUMS-net Model	99.91

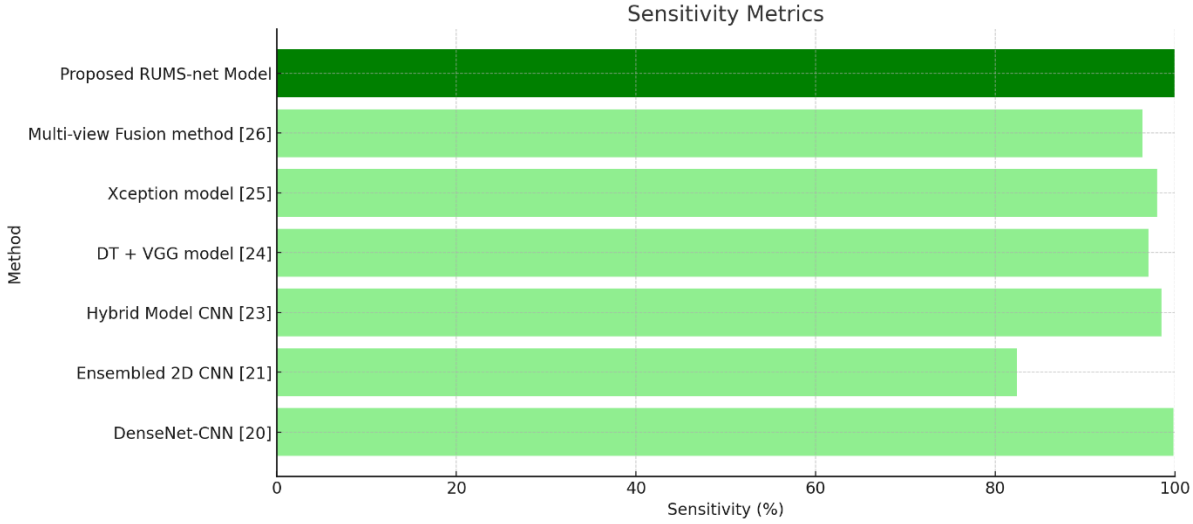

Fig. 20 Sensitivity Comparison

Table 4. Specificity Metrics

Method	Specificity
Ensembled 2D CNN [21]	93.9
Random Walker + Random Forest [22]	94.7
Hybrid Model CNN [23]	61.0
Xception model [25]	94.7
CNN Gradient Descent [27]	97.0
Proposed RUMS-net Model	98.23

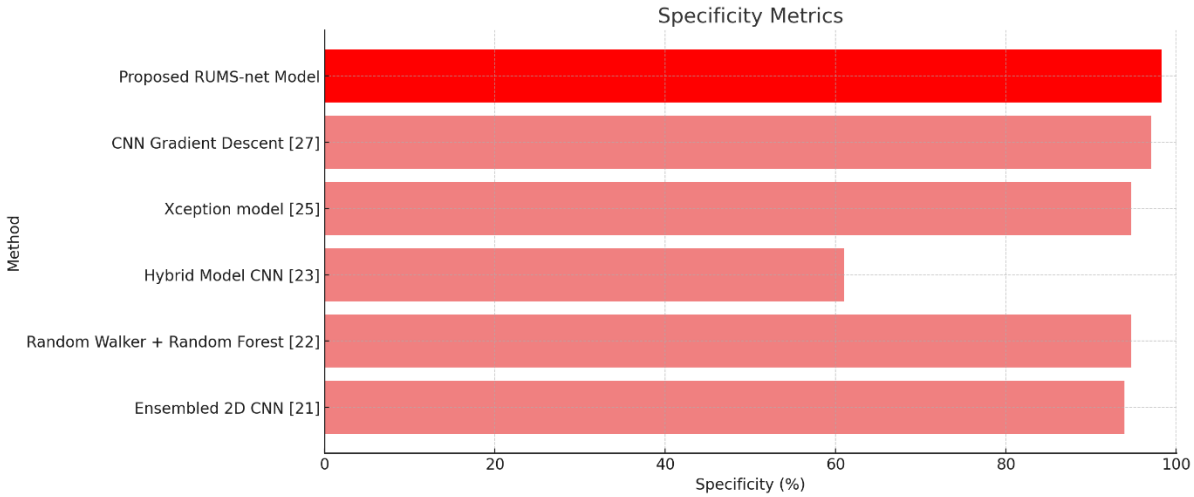

Fig. 21 Specificity Comparison

The sensitivity metrics, as outlined in Table 3, provide additional confirmation of the RUMS-net Model's strength, with a sensitivity rate of 99.91%. Figure 20 illustrates the sensitivity of different methods, emphasizing the exceptional sensitivity of the RUMS-net Model. The specificity metrics, as described in Table 4, quantify the model's capacity to accurately detect cases that are not cancerous. The RUMS-net Model demonstrates a specificity of 98.23%, as shown in Figure 21. The high specificity of this ensures a minimal number of false positives.

Table 5 Precision Metrics

Method	Precision
DenseNet-CNN [20]	99.20
Random Walker + Random Forest [22]	99.70
DT + VGG model [24]	94.00
Xception model [25]	94.80
CNN Gradient Descent [27]	96.39
Proposed RUMS-net Model	99.79

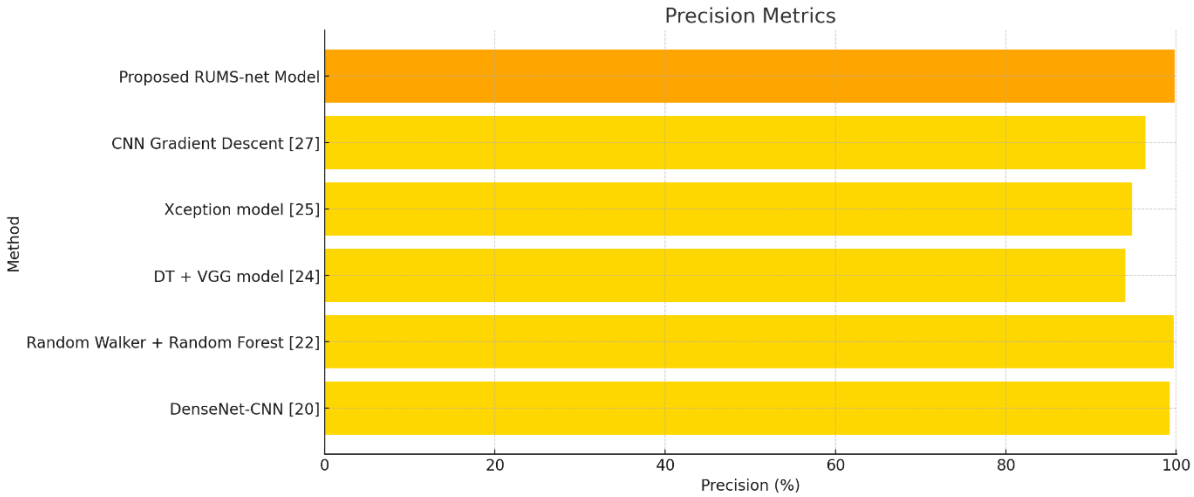

Fig. 22 Precision Comparison

The precision metrics, as shown in Table 5, evaluate the model's ability to correctly identify true positives. The RUMS-net Model demonstrates a precision rate of 99.79%, as depicted in Figure 22, highlighting its dependable ability to accurately classify instances of lung cancer. The thorough assessments validate the effectiveness of the RUMS-net Model in delivering accurate and dependable medical diagnosis and analysis.

5. Conclusion

Overall, the suggested methodology for processing and classifying lung cancer images using the RUMS-net model offers a thorough and highly efficient approach to analyzing medical images. The process commences by resizing the images to a uniform size of pixels using bicubic interpolation, guaranteeing consistency for subsequent processing stages. Subsequently, bilateral filtering is employed to decrease noise while retaining essential edge details, thereby upholding the integrity of anatomical structures in the images. Bi-Histogram Equalization (BBHE) greatly enhances image contrast, resulting in improved visibility of image features and better differentiation between different regions of interest. The iterative selection thresholding method transforms the enhanced images into a binary format, while maintaining crucial details and reducing interference from background noise. The binary images are further refined by performing morphological opening operations using disk-shaped structuring elements of different radii. This process eliminates small entities and smooths the outlines of larger structures. The binary images are inverted to facilitate active contour segmentation using the Random Walker algorithm, which precisely identifies object boundaries based on pixel intensity. By overlaying segmented outlines onto inverted images and implementing Wiener filtering, the amount of noise in the combined images is reduced, thus guaranteeing enhanced clarity. The following processes of binarization and hole-filling are used to remove background regions while retaining regions of interest for subsequent analysis. Circle detection is a technique used to identify areas of interest, such as tumors, by superimposing circles onto the original images, thereby improving the visual representation. The segmented image is obtained by subtracting binary images, and quantitative metrics such as the total area of the tumor and the ratio of affected area are calculated, which provide valuable data for diagnosis. The RUMS-net model utilizes ResNet-50 for feature extraction, U-Net for segmentation, and Multi-Class SVM for classification to accurately classify lung cancer. The model exhibits exceptional performance, attaining 99.75% accuracy, a sensitivity rate of 99.91%, a specificity rate of 98.23%, and a precision rate of 99.79%. The results highlight the dependability and efficiency of the RUMS-net model in precisely diagnosing and analyzing lung cancer. This comprehensive methodology guarantees accurate image processing and segmentation, while also offering strong classification capabilities, which greatly improves diagnostic accuracy. The exceptional performance of the RUMS-net model demonstrates its capacity to enhance patient outcomes through the provision of dependable and precise medical diagnoses. This contributes to the progress of medical imaging technology and the broader healthcare sector.

References

1. R. L. Siegel, K. D. Miller, H. E. Fuchs, and A. Jemal, “Cancer Statistics, 2021,” CA. Cancer J. Clin., vol. 71, no. 1, pp. 7–33, 2021, doi: 10.3322/caac.21654.
2. . Asuntha A (2016) PSO, genetic optimizationand SVM algorithm for lung cancer detection. J Chem Pharm Res 8(6):351–359 28.
3. Ahmad T, Shahnajparvin M (2020) Lung cancer detection using CT image based on 3D convolutional neural network. J Comput Comput Commun 8(3):35–48 29.
4. Chashmi AJ, Chehelamirani M (2019) Using adaptive median flter for noise removal from image to diagnose breast cancer. Merit Res J Eng 5:014–018
5. Kalaivani, N., Manimaran, N., Sophia, S., & Devi, D. (2020). Deep learning based lung cancer detection and classification. In IOP Conference Series: Materials Science and Engineering, vol. 994, (p. 012026). IOP Publishing.
6. . Dlamini Z, Francies FZ, Hull R, Marima R (2020) Artifcial intelligence (AI) and big data in cancer and precision oncology. Comput Struct Biotechnol J 18:2300–2311. https://doi.org/10.1016/j.csbj.2020.08.019. PMID:32994889; PMCID:PMC7490765 28.
7. Hendrix W, Hendrix N, Scholten ET, Mourits M, Trap-de Jong J, Schale- kamp S, Korst M, van Leuken M, van Ginneken B, Prokop M, Rutten M, Jacobs C (2023) Deep learning for the detection of benign and malignant pulmonary nodules in non-screening chest CT scans. Com- mun Med (Lond) 3(1):156. https://doi.org/10.1038/s43856-023-00388-5. PMID:37891360; PMCID:PMC10611755
8. Makaju, Suren, P. W. C. Prasad, Abeer Alsadoon, A. K. Singh, and A. Elchouemi. "Lung cancer detection using CT scan images." Procedia Computer Science 125 (2018): 107-114.
9. Available online: https://www.kaggle.com/datasets/raddar/nodules-in-chest-xrays-lidcidri
10. Hirsch FR, Scagliotti GV, Mulshine JL, Kwon R, Curran WJ Jr, Wu YL, Paz-Ares L. Lung cancer: current therapies and new targeted treatments. Lancet. 2017 Jan 21;389(10066):299-311.

11. Lemjabbar-Alaoui H, Hassan OU, Yang YW, Buchanan P. Lung cancer: Biology and treatment options. Biochim Biophys Acta. 2015 Dec;1856(2):189-210. doi: 10.1016/j.bbcan.2015.08.002. Epub 2015 Aug 19. PMID: 26297204; PMCID: PMC4663145.
12. Pass HI, Carbone DP, Johnson dH, Minna JD. Principles & practice of lung cancer: The official reference text of the iaslc. Wolters Kluwere: Lippincott williams and Wilkins; 2010.
13. Shtivelman E, Hensing T, Simon GR, Dennis PA, Otterson GA, Bueno R, Salgia R. Molecular pathways and therapeutic targets in lung cancer. Oncotarget. 2014;5(6):1392–1433.
14. . Bhatti UA, Tang H, Guilu W, Marjan S, Hussain A (2023) Deep learning with graph convolutional networks: an overview and latest applications in computational intelligence. Int J Intell Syst 2023:1–28. https://doi.org/10.1155/2023/8342104
15. Tekade R., Lung nodule detection and classification using machine learning techniques, Asian Journal for Convergence in Technology. (2018) 4.
16. Bhatti UA, Bazai SU, Hussain S, Fakhar S, Ku CS, Marjan S, Yee P, Jing L (2023) Deep learning-based trees disease recognition and classifcation using hyperspectral data. Comput Mater Continua 77:681–697
17. Billmeier SE, Ayanian JZ, Zaslavsky AM, Nerenz DR, Jaklitsch MT, Rogers SO. Predictors and outcomes of limited resection for early-stage non-small cell lung cancer. J Natl Cancer Inst. 2011 Nov 2;103(21):1621-9. doi: 10.1093/jnci/djr387. Epub 2011 Sep 29. PMID: 21960708; PMCID: PMC3206042.
18. Gierada DS, Black WC, Chiles C, Pinsky PF, Yankelevitz DF (2020) Low-dose CT screening for lung cancer: evidence from 2 decades of study. Radiol Imaging Cancer 2(2):e190058. https://doi.org/10.1148/rycan.2020190058. PMID:32300760; PMCID:PMC7135238
19. Petrella, Francesco. 2021. "Diagnosis and Treatment of Primary and Secondary Lung Cancers" Cancers 13, no. 3: 448.
20. Zhang, C., Aamir, M., Guan, Y. et al. Correction to: Enhancing lung cancer diagnosis with data fusion and mobile edge computing using DenseNet and CNN. J Cloud Comp 13, 111 (2024). https://doi.org/10.1186/s13677-024-00673-1
21. S., S. ., Parveen, N. ., Maqbool, A. ., Khan, H. ., Alghadeer, S. K. ., & Singh, G. . (2024). A Novel Approach for Lung Cancer Detection Using Deep Learning Algorithms. International Journal of Intelligent Systems and Applications in Engineering, 12(15s), 471–480.
22. Nair, Sneha S., V.N. Meena Devi, and Saju Bhasi. "Enhanced Lung Cancer Detection: Integrating Improved Random Walker Segmentation with Artificial Neural Network and Random Forest Classifier." Heliyon, vol. 10, no. 7, 15 Apr. 2024, article e29032. DOI: https://doi.org/10.1016/j.heliyon.2024.e29032.
23. Venkatesh, C., Chinna Babu, J., Kiran, A. et al. A hybrid model for lung cancer prediction using patch processing and deeplearning on CT images. Multimed Tools Appl 83, 43931–43952 (2024). https://doi.org/10.1007/s11042-023-17349-8
24. Krishna, S. Udit, A.N. Barath Lakshman, T. Archana, K. Raja, and M. Ayyadurai. "Lung Cancer Prediction and Classification Using Decision Tree and VGG16 Convolutional Neural Networks." The Open Biomedical Engineering Journal, 22 Apr. 2024, DOI: 10.2174/0118741207290271240322061032.
25. Chu, Phuong Thi Minh, Tram Pham Bich Ha, Ngoc Minh Vu, Hoang Ha, and Thu Minh Doan. "The Application of Deep Learning in Lung Cancerous Lesion Detection." medRxiv, doi: https://doi.org/10.1101/2024.04.12.24305708.
26. Nazir, Imran, Ihsan ul Haq, Salman A. AlQahtani, Muhammad Mohsin Jadoon, and Mostafa Dahshan. "Machine Learning-Based Lung Cancer Detection Using Multiview Image Registration and Fusion." Journal of Sensors, 16 Aug. 2023, https://doi.org/10.1155/2023/6683438.
27. Rajasekar, Vani, M.P. Vaishnnave, S. Premkumar, Velliangiri Sarveshwaran, and V. Rangaraaj. "Lung Cancer Disease Prediction with CT Scan and Histopathological Images Feature Analysis Using Deep Learning Techniques." Results in Engineering, vol. 18, June 2023, article 101111. https://doi.org/10.1016/j.rineng.2023.101111.
28. Rajput, Aayush, and Abdulhamit Subasi. "Lung Cancer Detection from Histopathological Lung Tissue Images Using Deep Learning." In Artificial Intelligence Applications in Healthcare & Medicine editorial, 2023, pp. 51-74. https://doi.org/10.1016/B978-0-443-18450-5.00008-6.